

Article

Evaluating the Performance of 193 nm Ultraviolet Photodissociation for Tandem Mass Tag Labeled Peptides

Mowei Zhou ¹, Ju Yeon Lee ^{2,3} , Gun Wook Park ^{3,†}, Neha Malhan ¹, Tao Liu ²  and Jared B. Shaw ^{1,*} 

- ¹ Environmental Molecular Sciences Laboratory, Pacific Northwest National Laboratory, Richland, WA 99354, USA; mowei.zhou@pnnl.gov (M.Z.); neha.malhan@pnnl.gov (N.M.)
- ² Pacific Northwest National Laboratory, Biological Sciences Division, Richland, WA 99354, USA; jylee@kbsi.re.kr (J.Y.L.); tao.liu@pnnl.gov (T.L.)
- ³ Research Center for Bioconvergence Analysis, Korea Basic Science Institute, Cheongju 28119, Korea; cancun@cellkey.co.kr
- * Correspondence: jared.shaw@e-msion.com
- † Current address: Bioinformatics Center, CellKey, Yongsan-gy 21312, Korea.
- ‡ Current address: e-MSion, Inc., Corvallis, OR 97330, USA.

Abstract: Despite the successful application of tandem mass tags (TMT) for peptide quantitation, missing reporter ions in higher energy collisional dissociation (HCD) spectra remains a challenge for consistent quantitation, especially for peptides with labile post-translational modifications. Ultraviolet photodissociation (UVPD) is an alternative ion activation method shown to provide superior coverage for sequencing of peptides and intact proteins. Here, we optimized and evaluated 193 nm UVPD for the characterization of TMT-labeled model peptides, HeLa proteome, and N-glycopeptides from model proteins. UVPD yielded the same TMT reporter ions as HCD, at m/z 126–131. Additionally, UVPD produced a wide range of fragments that yielded more complete characterization of glycopeptides and less frequent missing TMT reporter ion channels, whereas HCD yielded a strong tradeoff between characterization and quantitation of TMT-labeled glycopeptides. However, the lower fragmentation efficiency of UVPD yielded fewer peptide identifications than HCD. Overall, 193 nm UVPD is a valuable tool that provides an alternative to HCD for the quantitation of large and highly modified peptides with labile PTMs. Continued development of instrumentation specific to UVPD will yield greater fragmentation efficiency and fulfil the potential of UVPD to be an all-in-one spectrum ion activation method for broad use in the field of proteomics.

Keywords: quantitative proteomics; tandem mass tags (TMT); ultraviolet photodissociation (UVPD); glycopeptides; peptide fragmentation; mass spectrometry



Citation: Zhou, M.; Lee, J.Y.; Park, G.W.; Malhan, N.; Liu, T.; Shaw, J.B. Evaluating the Performance of 193 nm Ultraviolet Photodissociation for Tandem Mass Tag Labeled Peptides. *Analytica* **2021**, *2*, 140–155. <https://doi.org/10.3390/analytica2040014>

Academic Editor: Marcello Locatelli

Received: 2 September 2021

Accepted: 5 October 2021

Published: 9 October 2021

Publisher's Note: MDPI stays neutral with regard to jurisdictional claims in published maps and institutional affiliations.



Copyright: © 2021 by the authors. Licensee MDPI, Basel, Switzerland. This article is an open access article distributed under the terms and conditions of the Creative Commons Attribution (CC BY) license (<https://creativecommons.org/licenses/by/4.0/>).

1. Introduction

Mass spectrometry (MS)-based quantitative proteomics has been widely applied to measure protein concentrations and fold changes for probing regulatory mechanisms and understanding biological pathways in complex samples [1–3]. The essence of the measurement is based on correlations between the MS signal response of proteolytic peptide protein concentrations. To achieve high accuracy in quantitation, various labeling methods have been designed to introduce internal references. These methods primarily rely on the incorporation of stable isotopes that have indistinguishable chemical properties but distinct masses readily readable by MS. Samples labeled with different isotopologs can be mixed to yield a multiplexed sample that can be analyzed in a single MS experiment, greatly reducing analysis time.

Isobaric tags for relative and absolute quantification reagents (iTRAQ) [4] and tandem mass tag (TMT) [5] are among the most commonly used, commercially available reagents that introduce chemical modifications on proteolytic peptides. The tags are preferentially added to primary amines, including the peptide N-terminus and lysine side-chains. The

tags are composed of a mass reporter portion and a mass normalizer portion. The mass reporter portion of the tag is readily cleaved during peptide fragmentation to yield a reporter ion with a predictable mass, based on the type of ion activation method used. Reporter ions of different mass are created by varying a fixed number of heavy isotopes between the reporter and normalizer portions of the isobaric tags. Multiple samples can be each labeled by a different isobaric TMT reagent and then combined for liquid chromatography—tandem mass spectrometry (LC–MS/MS) analysis. Identical peptides from multiple samples will have the same mass after isobaric labeling and will be co-isolated for MS/MS. Yet, the reporter ions released from each sample show up at distinct m/z in the MS/MS spectra. This allows relative quantitation of peptides from multiple samples in a single spectrum and minimizes variations in instrument response. Additionally, the ability to multiplex a number of samples in the same LC–MS/MS experiment for relative quantitation significantly reduces the total time for high-throughput analysis of large quantities of samples. While sixplex labeling reagents are commonly used, higher order multiplexing reagents, such as TMT 10-, 11-, and 16-plex, for combining more than 6 samples [6–9] can also be achieved with high resolution mass spectrometers. Strategies of combining multiple orthogonal labeling reagents up to 27-plex have also been reported [10].

Collision-induced dissociation (CID) is the most widely used method for peptide fragmentation. In Orbitrap instruments, CID specifically refers to resonant excitation CID performed in ion traps. In tandem in space instruments, CID is equivalent to higher energy collision dissociation (HCD) in Orbitrap instruments. Due to differences in collisional energy regime, time scale, and detailed instrument design, they tend to access different fragmentation pathways [11]. However, all these methods fundamentally activate ions via gas collisions and increases in the internal energy of ions via vibrational excitation. TMT reagents have been designed to have labile bonds to CID/HCD to produce abundant reporter ions in MS/MS spectra. However, labile modifications such as glycosylation and phosphorylation can significantly alter the fragmentation behavior of peptides. CID/HCD tends to preferentially cleave labile modifications such as phosphorylation and glycosylation [12–14]. The spectra of these modified peptides typically lack sufficient peptide backbone fragments to sequence the peptides and localize the modification sites. For glycopeptides in particular, the cleavage of glycosidic bonds is the predominant fragmentation pathway. To confidently identify a glycopeptide, several features from the spectrum are needed. The oxonium ions in the low m/z region are indicators of the presence of glycans. The glycopeptide fragments with partially cleaved glycans are beneficial for assignment of glycan structures, and peptide backbone fragments are required to identify the peptide sequence. Typically, such information cannot be retrieved from a single fragmentation spectrum. Multiple CID/HCD spectra at different energies, stepped-HCD to cover different energy regimes, and alternating/hybrid activation methods have been developed to access additional fragmentation pathways for glycopeptide characterization [15–22].

Despite the important roles of glycoproteins in biology, they remain a very challenging class of molecules to study due to the high diversity and complexity of glycans, even with the latest analytical technology and methods [13]. The addition of TMT labeling creates another dimension complexity and further exaggerates the difficulties of glycopeptide characterization. Ye et al. performed a systematic study on TMT-labeled glycopeptides from bovine fetuin and reported that no reporter ions were generated in most spectra with online LC–MS/MS using HCD [23]. The lack of reporter ions using HCD normalized collision energies typical for unmodified peptides prevented effective quantitative analysis for N-glycopeptides by online LC–MS/MS. To overcome this issue, normalized collision energies of 40% [24] or even 70% [25], were necessary to obtain TMT reporter ions from N-glycopeptides. However, diagnostic ions for both the glycan and peptide structure were hardly detected in the spectra at such high HCD energies, and it may be difficult to identify unknowns in untargeted applications. An alternative solution is to deglycosylate (e.g., enzymatically for N-glycans) enriched glycopeptides to increase reporter ion signal, but glycan structural information is lost [26,27]. More recently, hybrid or multiple stage methods,

such as electron transfer dissociation (ETD) supplemented by HCD (EThcD), have shown promise for glycopeptide analysis [27,28], including TMT-labeled glycopeptides [29].

Development of new activation methods can greatly improve proteomics analysis, especially for those with labile modifications. Electron-based ion activation methods, in particular ETD, which is available in many commercial mass spectrometers, has been shown to fragment and sequence peptides while preserving labile modifications [12,30]. For TMT-labeled peptides, ETD cleaves the mass reporter at different locations compared to CID/HCD, yielding reporter ions with masses smaller by one carbon atom. Unfortunately, this eliminates one site for incorporating heavy isotopes in the reporter ions. Therefore, ETD is not fully compatible with commercial TMTduplex, TMT10plex and TMT11plex reagents, which all rely on the ^{13}C atom that is not retained in the reporter ion with ETD. Ultraviolet photodissociation (UVPD) has shown great promise in providing high sequence coverage while preserving labile modifications or even the site of charges for peptides and intact proteins [31–37]. Native proteins can also be fragmented by UVPD to obtain residue-specific structural information [38–41]. Recently it has manifested its potential for fragmenting O-glycopeptides [32,42]. However, to the best of our knowledge, there has been no previous report on the fragmentation behavior of TMT-labeled peptides by UVPD. In this work, we show that UVPD predominantly yields the same type of TMT reporter ions as CID/HCD. Mobile protons and peptides with relatively high numbers of acidic residues tend to have a higher propensity to yield spectra with missing TMT reporter ions. UVPD generally produces a wider variety of fragments than HCD and shows a lower percentage of matched spectra with missing TMT reporter ions. This feature can be very helpful for characterization of peptides with labile modifications, as demonstrated for glycopeptides. UVPD is not as effective for low abundance precursors due to its relatively low fragmentation efficiency. However, UVPD is an effective alternative for large and highly modified peptides with labile PTMs.

2. Materials and Methods

2.1. Materials

Glu-Fibrinopeptide B (GluFib) was purchased from Anaspec. TMTzero, TMTsixplex isobaric label reagents, and Pierce HeLa protein digest standard were purchased from Thermo Fisher Scientific. Alpha-1-acid glycoprotein (AGP) was purchased from Sigma Aldrich (G9885; Sigma Aldrich, St. Louis, MO, USA). AGP were denatured at 95 °C for 5 min, reduced with dithiothreitol (incubation at 60 °C for 1 h), alkylated with iodoacetamide, and trypsin digested to generate peptides for TMT labeling. All peptide samples were mixed with TMT reagents at a 1:10 weight ratio following the manufacturer's protocol. For TMTsixplex labeled HeLa samples, AGP digests and GluFib, all channels were mixed at equal amounts.

2.2. Liquid Chromatography–Mass Spectrometry (LC–MS/MS)

Waters NanoAcquity was coupled online with a Q Exactive HF mass spectrometer (Thermo Fisher Scientific, Waltham, MA, USA), which was modified to incorporate ultraviolet photodissociation, as described previously [35]. In the UVPD mode, ions stored in the HCD cell were irradiated by a user-defined number of laser pulses and pulse energy (193 nm ArF excimer laser, Coherent Inc., Santa Clara, CA, USA). C18 columns packed in-house (packing 3 μm Jupiter (Phenomenex, Torrance, CA, USA), column ID 75 μm , OD 360 μm , length 70 cm) were used for reversed-phase liquid chromatography separations. Mobile phase A was 0.1% formic acid in water and mobile phase B was 0.1% formic acid in acetonitrile. A 5 cm, 150 μm i.d. trapping C18 column was used to desalt the sample online with 1% mobile phase B for 10 min before the analytical gradient. For HeLa digests, the gradient of mobile phase B started from 1% and increased to 3%, 8%, 25%, 50% at 2, 30, 200, 240 min, respectively. The column was washed with 95% mobile phase B for 5 min at the end of the gradient and then equilibrated at 1% mobile phase B for 30 min. An estimated 0.2 μg of peptides were used for each injection. For AGP digests, the gradient

was compressed into 100 min, and 0.5 µg peptides were injected each time. The flow rate on the LC was 0.3 µL/min, with a nanoelectrospray voltage of 1.8–2.0 kV and a capillary temperature of 275–300 °C. MS spectra were acquired at 60 K resolution with an AGC target of 1E6 and a maximum injection time of 20 ms. MS/MS spectra were taken at 15 K resolution with an AGC target of 1E5 and a maximum injection time of 100 ms. Precursors were isolated with a 1 *m/z* window, except for initial dataset for optimizing energies, which was with a 2 *m/z*. Dynamic exclusion was set to 10 s. Unassigned and singly charged ions were excluded for fragmentation. HCD energies, UVPD laser energy and laser pulse number were varied, as discussed in the results.

2.3. Data Analysis

HeLa LC–MS data were processed with MSGF+ [43] by searching against human proteins. Peptide-spectrum matches (PSMs) with a probability score below 1E-8 were selected and further processed with MASIC and MASICResultsMerger [44] to extract the associated intensities of TMT reporter ions. The results were filtered to allow only one PSM per spectra (removing duplicate PSMs of the same peptide from homologous proteins sharing the same sequence segments). Results were visualized and peptide coverage maps were generated in LcMsSpectator [45].

TMT-labeled AGP data were processed by Byonic (Protein Metrics Inc., Cupertino, CA, USA) and Integrated GlycoProteome Analyzer (I-GPA) [21]. N-glycopeptides were identified and manually checked based on I-GPA results. The workflow is briefly explained as follows. First, N-glycopeptide tandem MS/MS spectra, including oxonium ions, based on a 15 glycan-specific reference were selected. Second, if their experimental MS isotope patterns were matched to the theoretical patterns of N-glycopeptides in the glycan database, they were selected as N-glycopeptide candidates. The database in I-GPA (referred to as GPA-DB) is composed by combining possible tryptic peptides including N-glycosites of AGP and 351 N-glycans (331 retrosynthetic glycans from Kronewitter et al. [46], and 20 glycans of penta- and hexa-poly-lactosamine series from Ozohanics et al. [47]). Finally, N-glycopeptides of AGP were identified by their Y-score upon matching of experimental and theoretical fragments. To calculate Y-scores, fragments from both peptide bond cleavages and glycosidic bond cleavages were considered. The I-GPA search parameters were: missed cleavages (=0) and fixed modification of carbamidomethyl cysteine and mammalian N-glycan. Additionally, TMT-labeling modifications were considered for N-terms and lysines. The mass tolerances for precursor and fragment ions were set at 0.02 Da. N-glycopeptides with a Y-score above 60 were validated and filtered based on the previously identified N-glycopeptides from AGP [48].

3. Results and Discussion

3.1. UVPD Primarily Generates CID/HCD Type Reporter Ions for TMT-Labeled Peptides

To evaluate the types of TMT reporter ions in UVPD, we first performed TMT6 labeling on pure GluFib peptide, infused into the MS at 0.01 mg/mL in 50% ACN and 0.05% formic acid. UVPD (2 mJ, 2 pulses) and HCD (55 V) of the labeled GluFib peptide (doubly charged) shared identical fragments in the low mass region corresponding to the standard TMT6 126–131 ions observed for HCD (Figure 1a,d). It is noted that methyl loss from TMT6 126–131 reporter ions led to the formation of reporter ions in the *m/z* range of 112–117, which were detected at about 3% intensity relative to the 126–131 ions (Figure 1b, intensity magnified by 5). Other common fragments in the *m/z* range of 112–116 are likely related to immonium ions (Figure 1b,e). Trace levels (~0.1% of 126–131 reporters) of ETD type reporter ions were also seen in the UVPD spectrum (not shown). ETD-type reporter ions are not ideal for TMT with high levels of multiplexing, because the different cleavage site in ETD eliminates one carbon atom from an additional labeling site (incompatible with commercial TMT2 and TMT10). Both UVPD and HCD yielded full sequence coverage of the peptide while generating identical reporter ions for relative quantitation. The signal

levels for TMT ions were similar in UVPD and HCD (5E6~6E6). UVPD had a higher signal for the unfragmented precursor (Figure 1c,f).

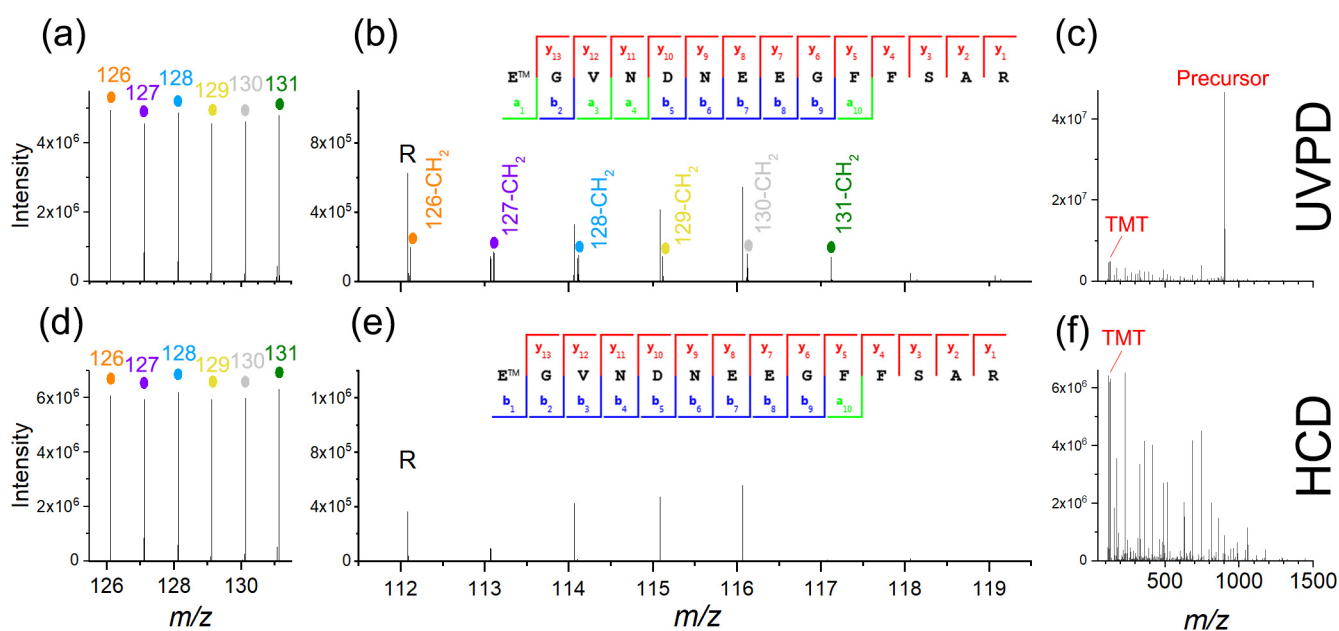


Figure 1. Low mass fragments of TMTsixplex reporter ions with (a–c) UVPD and (d–f) HCD for Glu-Fibrinopeptide B. The first two columns are zoomed onto a low m/z region for better display of reporter ions. (c,f) show the full spectra. Peak intensities are labeled on the y axes. Inserts in (b,e) show the peptide coverage based on observed fragments in the full spectra.

3.2. Effects of UVPD Energy and Laser Pulses on TMT-Labeled Peptides

UVPD parameters were optimized by exploring the impact of laser pulse energy (1 mJ, 2 mJ, 3 mJ) and the number of pulses (1 pulse or 2 pulses) on HeLa digests labeled with TMT6, with each channel mixed at equal concentrations. We also chose 3 normalized collision energies (NCEs) of HCD: 23%, 28%, and 33% for comparison. The total numbers of MS/MS spectra were similar across all conditions, except for ~10% decrease for UVPD 2 mJ 3 pulses (Figure 2a, gray bars), likely due to longer acquisition times from high numbers of laser pulses. Total peptide-spectrum matches (PSMs) were both optimized at relatively high activation energies (Figure 2a, white bars). Identifications were maximized at 28 or 33 NCE, and 2 mJ 2 pulses or 3 mJ 1 pulse for HCD and UVPD, respectively. It is interesting to note that 2 mJ 1 pulse performed better than 1 mJ 2 pulses, although the total energy inputs are both 2 mJ. In addition, the experiments with 2 mJ 3 pulses (6 mJ total) did not perform better than 2 mJ 2 pulses (4 mJ total) or 3 mJ 1 pulse (3 mJ). These results suggest that more pulses and higher total energy input may not necessarily help in obtaining more identifications in UVPD, either because of over-fragmenting of peptides into secondary fragments or reduced speed with the high number of pulses.

Among the optimized conditions for HCD and UVPD where the numbers of PSMs were maximized, we observed 2% of PSMs with missing TMT reporter ions (at least one of the 6 channels were not detected) for HCD NCE 28%, despite a similar number of PSMs to HCD NCE 33%, where only 0.2% PSMs were missing reporter ions (Figure 2b). This indicates that the HCD fragmentation can be “incomplete” even though sufficient fragments can be obtained for identifying the peptide. At UVPD conditions with a total energy input of no less than 3 mJ (2 mJ 2 pulses, 2 mJ 3 pulses, and 3 mJ 1 pulse), PSMs/peptides that are missing reporter ions are less than 0.1%. In order to evaluate the quantitation performance, we also calculated the coefficient of variation (CV) of the relative ratio of reporter ions (average of channel 126–130 to 131 per PSM, Figure 2c). The CV of quantitation results obtained from the average intensity ratios of reporter ions decreased with increasing energy

input for both HCD and UVPD. This trend is as expected as the intensities of reporter ions grew at higher energies, resulting in less variability and better statistics for quantitative measurement. We also evaluated the quantitation performance of UVPD by spiking known concentrations of digested peptides in each TMT channel (difference of concentrations over 10-fold), which showed very similar results and quantitation accuracy to HCD (data not shown).

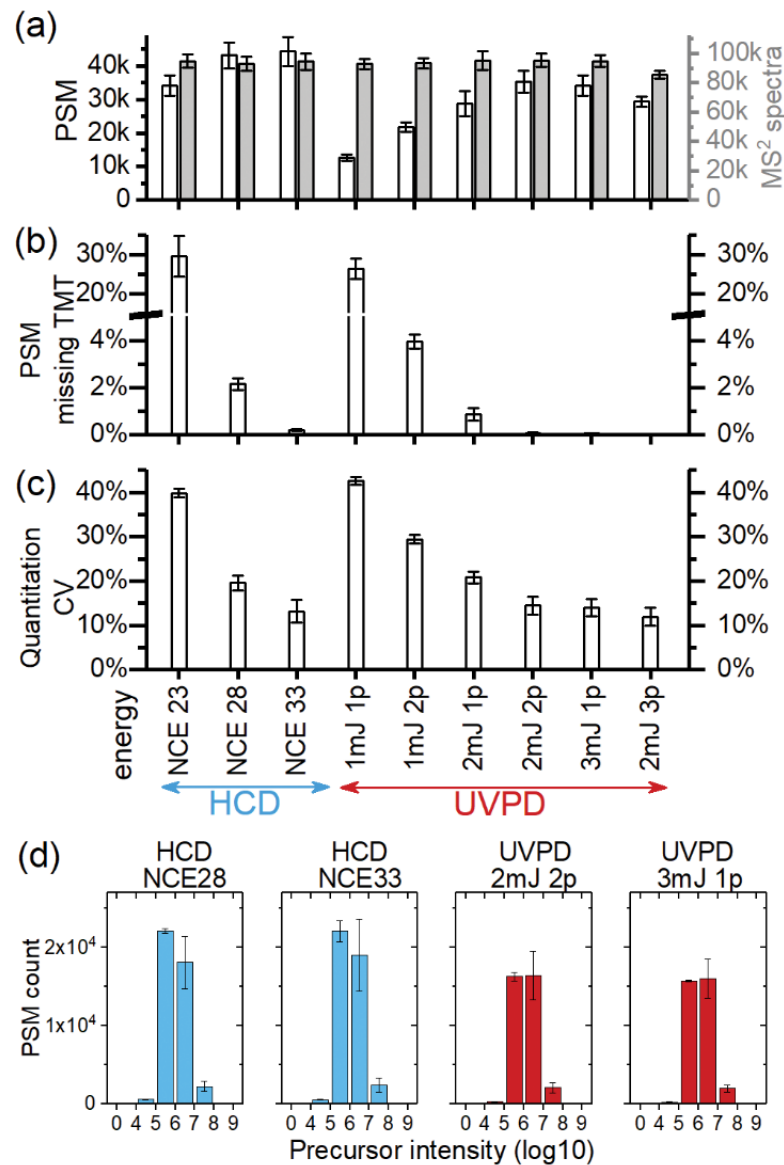


Figure 2. Optimization of peptide identifications and TMT quantitation performance for HCD (left 3 on x axis in (a–c)) and UVPD (right 6 on x axis in a–c) by varying activation energies. **(a)** Total PSM (left y axis, white bars) and total number of MS² spectra (right y axis, gray bars). **(b)** Percentage of PSMs that have at least one missing reporter ion. A break in the y axis is introduced at 5–15% to better display the values < 5%. **(c)** Average CV of relative quantitation for channel 126–130 to channel 131, excluding PSMs with at least one missing reporter ion. Data from 3 technical replicates were merged within each energy condition. **(d)** Histograms showing the precursor intensity distributions of PSMs for the optimized conditions of HCD NCE 28, HCD NCE 33, UVPD 2 mJ 2 pulses, and UVPD 3 mJ 1 pulse. Error bars in (a,b,d) are the standard deviations of 3 technical replicates. Error bars in (c) are the standard deviation of relative quantitation of the 5 channels.

Overall, optimal performance for TMT-labeled HeLa peptides using 193 nm UVPD was observed at 2 mJ 2 pulses and 3 mJ 1 pulse. However, even under optimized conditions, the total PSMs and the number of unique peptides in UVPD are still about 80% of those for HCD. This is likely a result of the relatively high absolute intensity of the remaining precursor ions and the low absolute intensity of the fragment ions in UVPD. To confirm this, we examined the distribution of precursor ion intensities for all the PSMs under optimized HCD and UVPD conditions (Figure 2d). There is a disproportionately higher number of PSMs from precursors at an intensity of 1×10^5 for HCD than for UVPD. This highlights the challenges associated with the relatively low abundance of product ions in UVPD spectra, and is the major obstacle for improving PSMs by UVPD for low absolute abundance peptides in high-throughput LC-MS/MS experiments. Developments in instrumentation are also expected to increase the relative abundance of fragment ions in UVPD and further improve the number of identifications [49]. Alternatively, chemical labels with chromophores that absorb strongly at specific wavelengths can be utilized to improve UVPD to selectively target certain classes of peptides in shotgun proteomics [50,51].

3.3. The Tendency of Missing TMT Reporter Ions Also Correlates with Peptide Sequence

PSMs with missing reporter ions are problematic for quantitative analysis, especially if the peptides are important biomarkers of interest. Although HCD NCE 28% showed optimum PSM counts, a significant portion of the PSMs had missing TMT reporter ions. There were also PSMs with no reporter ions at all (data not shown). After manually checking some of these spectra, it was found that many of the PSMs with missing reporter ions contained high signal to noise backbone cleavage fragment ions and yielded confident identification, yet no reporter ions were released. Therefore, we investigated the peptide sequences of the PSMs missing reporter ions to find sequence-dependent behavior. While HCD primarily generates b/y ion types from vibrational excitation, 193 nm UVPD is known to generate additional ion types including a/x and c/z, some of which are believed to be from electronic excitation [52]. It has been well documented in collision-induced activation that protons have to be located to side-chains to imitate charge-directed backbone cleavages to generate b/y ions. Without mobile protons, the charges are sequestered on basic residues, and thus higher energy is required to mobilize the protons to produce fragmentation [53]. We counted the number of “mobile protons” (Figure 3) in the peptides for each PSM and compared the distribution of the counts between all PSMs and the PSMs missing reporter ions. Although peptide N-termini and lysine residues are expected to be completely labeled with TMT tags, the tertiary amine in the TMT has high gas phase basicity [54] and can sequester a proton. Thus, we define the number of “mobile protons” here as the peptide charge minus the sum of the N-terminus and the total number of lysine and arginine residues.

Overall, most peptides have either zero or one mobile proton. For all PSMs (Figure 3a–i, upper panels), lower activation energies generally yielded fewer PSMs for peptides with zero mobile protons; while at higher activation energies the ratio of PSMs for peptides with zero mobile protons increased. The ratios of PSMs with zero mobile protons (counts equal to or less than 0) to those with mobile protons (counts equal to or more than 1) showed exponential growth with increasing activation energies for both UVPD (Figure 3j) and HCD (Figure 3k). This indicates that higher energy is required to generate sufficient fragments for peptides without mobile protons. Although UVPD conditions of 2 mJ 1 pulse and 1 mJ 2 pulses had the same total energy input, the lower power of 1 mJ 2 pulses was not as effective as 2 mJ 1 pulse for fragmenting peptides with no mobile protons. This is consistent with the fewer PSMs for UVPD with multiple, low energy pulses (Figure 2). It is possible there was insufficient excess energy to be redistributed to vibrational modes to break the noncovalently associated peptide fragments. For PSMs with missing TMT (Figure 3, lower panels), the distribution was biased towards peptides with 1 or more mobile protons regardless of activation conditions. Even at high activation energies where the sample sizes were small, the PSMs for peptides with one mobile proton

still dominated the histogram (except for UVPD 2 mJ 3 pulses where only 4 PSMs were missing TMT, Figure 3g). This implies that peptides with mobile protons may have a higher likelihood of accessing non-residue specific cleavages, thus lowering the probability of cleavage occurring at the TMT tag to release the reporter ions.

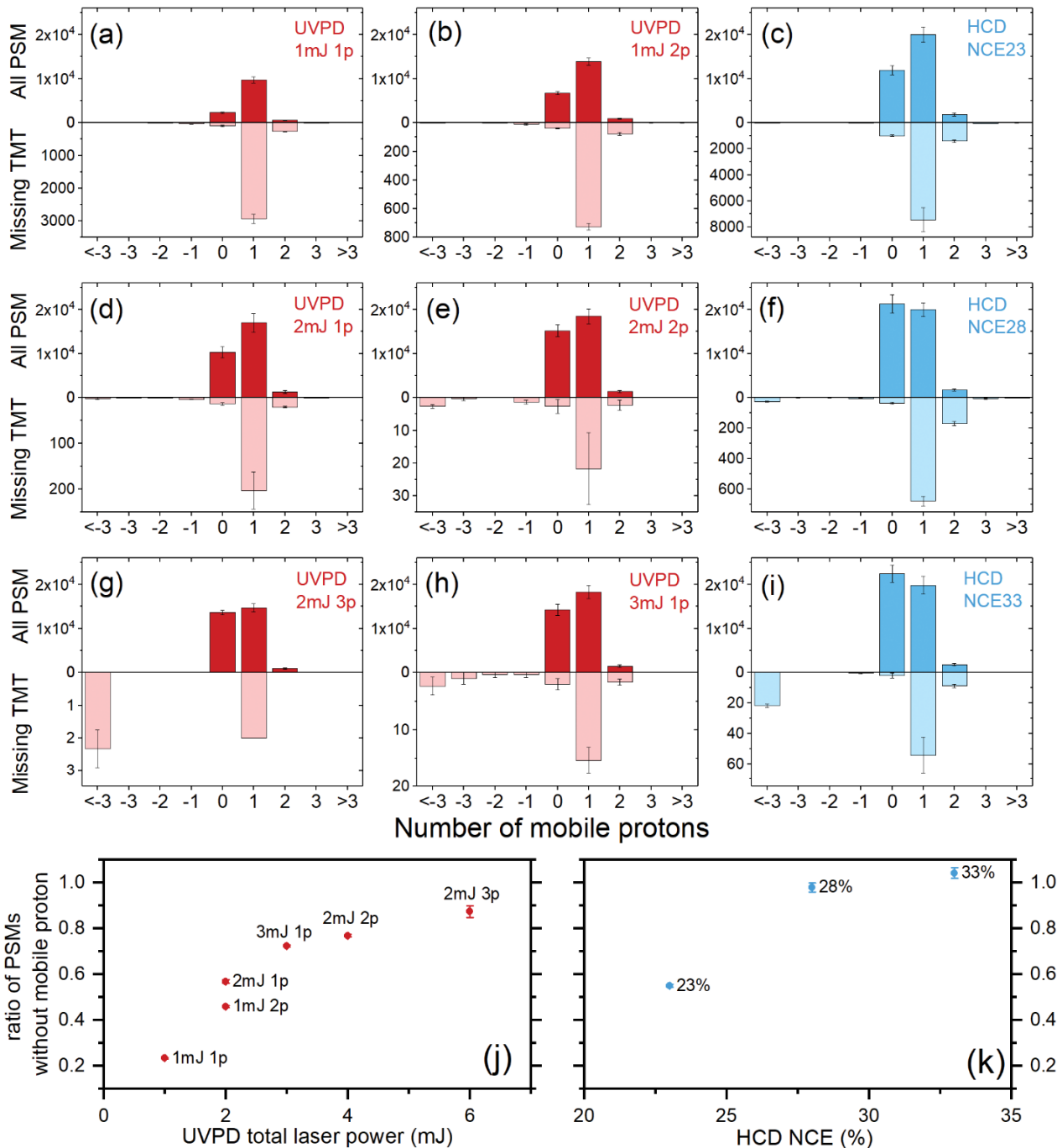


Figure 3. Histograms of the number of mobile protons for PSMs under different (a,b,d,e,g,h) UVPD and (c,f,i) HCD activation conditions, as noted in the top right corner of each plot. For each plot in (a–i), the upper panel is the histogram for all PSMs, while the lower panel is for the PSMs with missing TMT reporter ions. All upper panels were set to the same scale for easy comparison. All lower panels were scaled differently for full display of the distribution even for very low counts. (j) Ratio of PSMs with no mobile protons to PSMs with mobile protons as a function of total UVPD laser power and (k) HCD NCE. Laser pulse energy, the number of laser pulses, and NCE are labeled next to the data points. All error bars are from 3 technical replicates.

We also examined the distribution of the number of acidic residues in the PSMs, because aspartic acid and glutamic acid residues are known to be the preferred cleavage sites for collisional activation in the absence of mobile protons [53]. Most PSMs are from peptides with 2–3 acidic residues (Figure 4, upper panels), and there are no distinct differences in their distribution across all UVPD and HCD conditions. For PSMs with missing TMT, a bias for peptides with more acidic residues was noticeable for UVPD 1 mJ 1 pulse (Figure 4a, lower panel), 1 mJ 2 pulses (Figure 4b, lower panel), and HCD 23% (Figure 4c, lower panel), as shown by the slight shift of the apex of the histograms to 2–3 acidic residues. The bias was also visible in UVPD 2 mJ 1 pulse (Figure 4d, lower panel), and it became most obvious for HCD 28% (Figure 4f, lower panel), which showed a strong preference for peptides with 4 acidic residues. At higher activation energies (Figure 4e,g–i) the distributions became more random without clear patterns, partially because of the low number of PSMs with missing TMT at high activation energies. Among the optimized conditions for UVPD and HCD (Figure 4e,f,h,i based on maximum PSM counts in Figure 2), only HCD 28% showed a bias for PSMs from peptides with high numbers of acidic residues to have missing TMT ions. These observations can be explained by the preferred cleavage of C-terminal to acidic residues with limited activation energies, thus reducing the chance of generating reporter ions. The difference between HCD 28% and HCD 33%, despite the similar total number of PSMs, further illustrated that sequence-dependent preferential cleavage in HCD may lead to missing of TMT and incomplete quantitation. The results from this analysis indicate that fragmentation of TMT-labeled peptides by 193 nm UVPD is also affected by amino acid sequence, as described in the mobile proton model, which was developed from collisional activation. This implies that 193 nm UVPD and HCD share, at least partially, common fragmentation pathways due to the conversion of electronic excitation into vibrational modes.

3.4. UVPD for TMT Glycopeptides

The performance of UVPD for TMT-labeled glycopeptides was evaluated by comparing the results of AGP peptides using an Integrated GlycoProteome Analyzer (I-GPA) (Figure 5). The number of confident glycopeptide PSMs peaked at around 300 for UVPD 3 mJ 1 pulse and 2 mJ 2 pulses. HCD, similarly to the previous results on unmodified peptides, showed a higher number of total glycopeptide PSMs, which peaked at around 550 at NCE 23 and 28. However, many of the HCD spectra showed missing TMT reporter ions, because the glycosidic bonds were the most labile and were preferentially cleaved before the TMT reporter ion. After filtering out spectra with missing TMT, the quantifiable PSMs turned out to be similar between the best HCD (NCE 33) and UVPD (3 mJ 1 pulse, and 2 mJ 2 pulses) conditions (Figure 5b). Although HCD NCE 28 was able to produce ~80 quantifiable PSMs, the variation of the quantitation was significantly higher than the best HCD and UVPD conditions, as shown by the CV in Figure 5c. The results showed the necessity of using relatively high energy to obtain the best quantitation performance for TMT-labeled glycopeptides. Unfortunately, the HCD condition of NCE 33 that generates the best quantification data is not the optimal condition for identifying glycopeptides, as shown by the lower total glycopeptide PSMs compared to NCE 28 and NCE 23 in Figure 5a. This is because high HCD energies produced spectra that were dominated by oxonium ions in the low m/z range and reduced the ions of high m/z range which are needed for confident glycopeptide identification. Although the UVPD methods need further development to improve the total number of PSMs (mostly for low abundance peptides), the UVPD spectra generally show a wide variety of fragments under a single condition, that provide sufficient information for both characterization and quantitation.

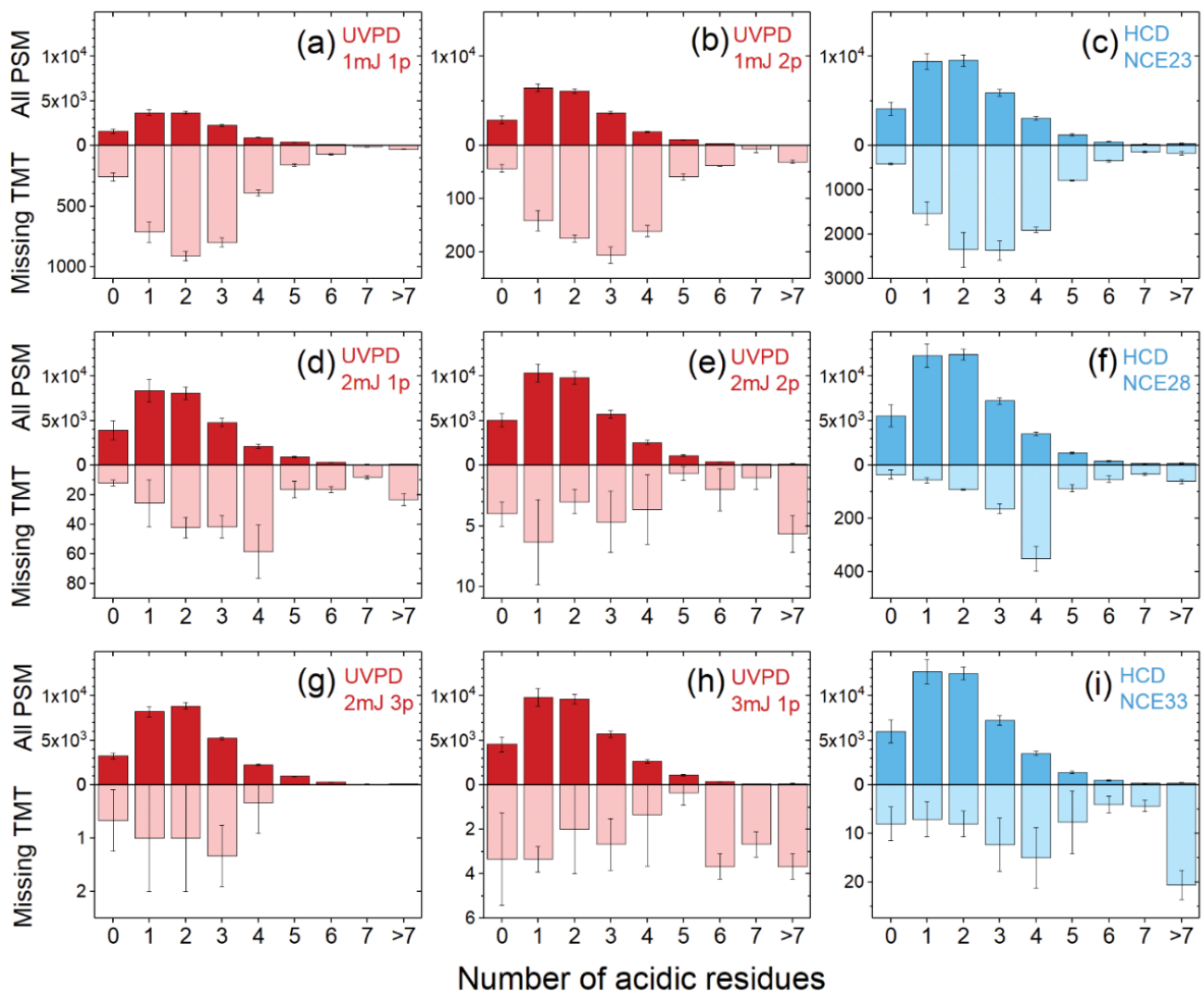


Figure 4. Histograms of the number of acidic residues for PSMs under different (a,b,d,e,g,h) UVPD and (c,f,i) HCD activation conditions, as noted in the top right corner of each plot. For each plot, the upper panel is the histogram for all PSMs, while the lower panel is for the PSMs with missing TMT reporter ions. Error bars are from 3 technical replicates. All upper panels were set to the same scale for easy comparison. All lower panels were scaled differently for full display of the distribution even for very low counts.

We manually examined the spectra for identified glycopeptides under the conditions that gave the largest number of PSMs (NCE 28 for HCD, 3 mJ 1 pulse for UVPD). One example glycopeptide, LVPVPITNATLDQITGK (6Hexose + 5HexNAc + 3NeuAc), is shown in Figure 6a,b. We noticed several different patterns between the two fragmentation methods. The first difference is in the oxonium ions, which are critical for glycopeptide identification. The oxonium ions of 366.140 from 2 glycans (Hexose + GlcNAc) are among the strongest fragments in both HCD and UVPD. However, in the HCD spectrum, the intensity of the oxonium ions from one glycan (138.0555 from GlcNAc-2H₂O-CH₂O, 168.0661 from GlcNAc-2H₂O, 186.0766 from GlcNAc-H₂O, 204.0872 from GlcNAc, 274.0927 from NeuAc-H₂O and 292.1032 from NeuAc) are stronger than those from 3 glycans (528.1928 from GlcNAc + 2 Hexose and 657.2354 from GlcNAc + Hexose + NeuAc) or 4 glycans (819.2870 from GlcNAc + 2Hexose + NeuAc). In contrast, the oxonium ions from 2, 3 and 4 glycans in UVPD are more intense than those from one glycan. Second, the information of glycan-cleaved glycopeptide fragments for the characterization of a glycan structure from a glycopeptide is different. There were higher numbers of glycopeptide fragments retaining larger

portions of the glycan in UVPD than in HCD (labeled peaks $> m/z$ 700 in Figure 6b), allowing the assignment of almost the whole glycan composition from precursor N-glycopeptide. The glycans of glycopeptide fragment ions from HCD instead generally only retained core glycans in a peptide (PEP + GlcNAc, PEP + 2GlcNAc and PEP + 2GlcNAc + Hexose in Figure 6a). Third, for peptide fragments, which identify the amino acid sequence of a glycopeptide, UVPD generates a/x and c/z ions in addition to the b/y ions seen in HCD. Therefore, the number of peptide fragments from UVPD is more than that from HCD and results in identification of the amino acid sequence of glycopeptides with confidence. For HCD NCE 17% (Figure 6c), the distribution of the oxonium ion intensities was similar to UVPD, and the information on glycan-cleaved glycopeptide fragments is more than from HCD NCE 28% but not as much as from UVPD. The intensity of TMT reporter ions is poor from HCD NCE 17%.

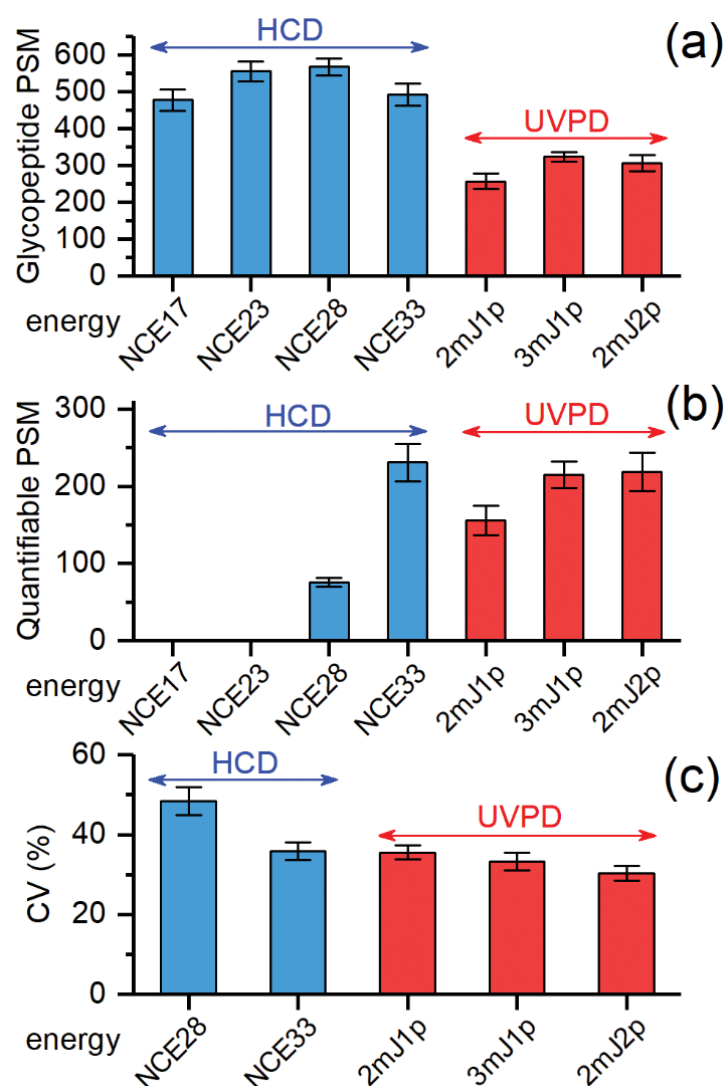


Figure 5. Comparison of different HCD (blue columns) and UVPD (red columns) energies for analysis of TMT6-labeled AGP glycopeptides using I-GPA. The numbers of glycopeptide PSMs are shown in (a). The counts of quantifiable glycopeptide PSMs, which have no missing TMT channels, are shown in (b). Error bars in (a,b) are from 3 technical replicates. (c) Average CV of relative quantitation for channel 126–130 to channel 131 for quantifiable PSMs, with standard deviation of relative quantitation of the 5 channels shown as error bars.

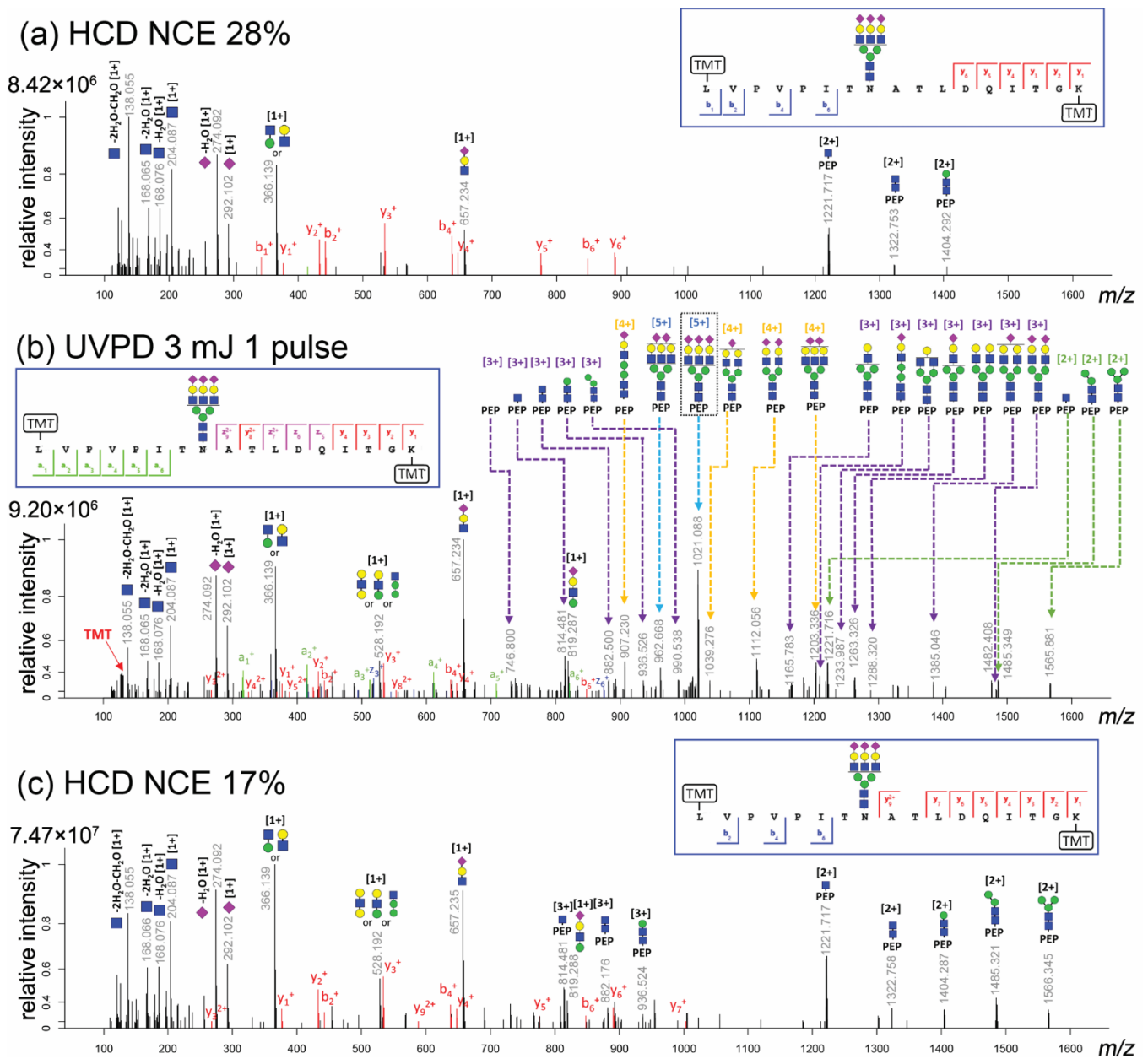


Figure 6. MS/MS spectra of a representative N-glycopeptide of TMT-labeled AGP identified from (a) HCD NCE 28%, (b) UVPD 3 mJ 1 pulse, and (c) HCD NCE 17%. Peptide backbone fragments are colored, with assignments labeled on the peaks (a/b/c/x/y/z). Glycan oxonium ions and intact peptide ions with partially cleaved glycans are labeled with their m/z values and cartoon structures. Intact peptide was simplified as “PEP” in the labels. The glycan structure annotation follow the nomenclature of the Consortium for Functional Glycomics [55]. The precursor glycopeptide sequences and coverage maps are shown in the blue boxes. Remaining precursors were not seen in the HCD spectrum but was observed in UVPD as highlighted by the dotted black box in (b). UVPD generates a wide variety of fragments, including a complete set of TMT reporter ions. UVPD provided better coverage of the glycans than HCD at a single energy. Note that MS/MS spectra were taken from similar retention times and the same precursor for best comparability (see scan numbers in raw data in the Data Availability Statement). The absolute signal levels were shown above the y axis in each spectrum.

The differences in fragmentation observed between UVPD and HCD were generally observed throughout the glycopeptide datasets. Successful identification of N-glycopeptides requires peptide fragments, glycan-cleaved glycopeptide fragments, and oxonium ions [48]. Based on this, UVPD provides more confident results than HCD for the identification of N-glycopeptides, because the number of glycan-cleaved glycopeptide

fragments, for information on glycan structures, and the number of peptide backbone fragments, for the characterization of the amino acid sequences, is greater from UVPD than from HCD. But the total number of N-glycopeptides identified from UVPD is less than from HCD because of the low fragment efficiency of UVPD containing unfragmented precursor ions. The fragment ions from HCD spectra had been well matched for identifying glycopeptides, but fragment ions matched from HCD spectra are not enough to assign the full glycan structure. Low HCD energies yielded more glycan-cleaved glycopeptide fragments, but also significantly reduced the intensities of TMT reporter ions for quantitative analysis. Therefore, combining HCD at different energies [18,23], or using stepped-energy HCD [17,20] (single spectrum acquired with fragments from different energies) can be beneficial for TMT-labeled glycopeptides. In contrast, the optimized condition of UVPD for glycopeptides was able to access many different fragmentation pathways such as those of oxonium, glycan-cleaved glycopeptide and peptide fragment ions and quantifiable TMT reporter ions with a single pulse energy.

4. Conclusions

Our data showed that UVPD of TMT-labeled peptides generated primarily the same type of reporter ions as HCD. It was also discovered that peptides containing mobile protons have a high propensity to yield spectra with missing channels of reporter ions. High numbers of acidic residues also contributed to missing TMT ions. These trends applied to both HCD and UVPD, suggesting that the two activation methods should share some common fragmentation mechanisms. For TMT-labeled N-glycopeptides, UVPD generally produced more types of fragments at glycosidic bonds than HCD. The wider range of cleavages at glycosidic bonds in UVPD provided more fragments to map the glycan structures for confident identification. At the same time, UVPD showed more consistent detection of TMT reporter ions (fewer missing values) than HCD for the TMT-labeled N-glycopeptides. Despite an overall higher coverage in UVPD spectra, the total number of PSMs in UVPD is consistently lower than that in HCD. This is likely because of the difficulties in detecting low intensity fragment ions, especially from low abundant precursors. Future developments would potentially address these issues and enable UVPD as a complementary tool for proteomics applications, especially for peptides with labile PTMs. In addition, there is ongoing interest in labeling intact proteins with isobaric tags for better quantitation in top-down proteomics [56]. UVPD fragmentation efficiency increases with the size of peptides/proteins because of higher photon absorption efficiency. Therefore, we also expect UVPD to improve quantitation and characterization of TMT-labeled large peptides and proteins in middle-down and top-down proteomics.

Author Contributions: Conceptualization, J.B.S. and M.Z.; formal analysis, M.Z., J.Y.L., G.W.P. and J.B.S.; investigation, M.Z., J.Y.L., N.M., J.B.S., writing—original draft preparation, M.Z., writing—review and editing, M.Z., J.B.S., J.Y.L. and T.L.; funding acquisition, J.B.S. and T.L. All authors have read and agreed to the published version of the manuscript.

Funding: Portions of this research were supported by a U24CA210955 grant from the U.S. National Cancer Institute's Clinical Proteomic Tumor Analysis Consortium (CPTAC), the National Research Foundation of Korea (NRF) grant funded by Korea government (MSIT) (No. 2021R1F1A1061840), and a grant from the Korea Basic Science Institute (KBSI) (Research Grant No. C170100).

Institutional Review Board Statement: Not applicable.

Informed Consent Statement: Not applicable.

Data Availability Statement: Raw data were deposited to MassIVE (<https://massive.ucsd.edu>; uploaded 31 August 2021) with identifier MSV000086049. MSGF+ and Byonic results were included. Spectra shown in Figure 6 are from "20180611TMTAGP_HCD28c.raw" scan number 41765, "20180611TMTAGP_UVPDe3p1c.raw" scan number 41716, and "20180611TMTAGP_HCD17a.raw" scan number 41648, respectively.

Acknowledgments: We thank Ernesto Nakayasu, Tujin Shi, and Chia-Feng Tsai for helpful discussions; Matt Monroe for helping with the software and data deposition. This work was performed at the Environmental Molecular Science Laboratory (EMSL), a DOE Office of Science User Facility sponsored by the Office of Biological and Environmental Research and located at the Pacific Northwest National Laboratory, and this work was partially funded by the high-resolution mass accuracy capability project.

Conflicts of Interest: The authors declare no conflict of interest. The funders had no role in the design of the study; in the collection, analyses, or interpretation of data; in the writing of the manuscript, or in the decision to publish the results.

References

1. Schubert, O.T.; Röst, H.L.; Collins, B.C.; Rosenberger, G.; Aebersold, R. Quantitative proteomics: Challenges and opportunities in basic and applied research. *Nat. Protoc.* **2017**, *12*, 1289–1294. [[CrossRef](#)] [[PubMed](#)]
2. Pappireddi, N.; Martin, L.; Wühr, M. A Review on Quantitative Multiplexed Proteomics. *ChemBioChem* **2019**, *20*, 1210–1224. [[CrossRef](#)] [[PubMed](#)]
3. Cifani, P.; Kentsis, A. Towards comprehensive and quantitative proteomics for diagnosis and therapy of human disease. *Proteomics* **2017**, *17*, 1600079. [[CrossRef](#)]
4. Ross, P.L.; Huang, Y.N.; Marchese, J.N.; Williamson, B.; Parker, K.; Hattan, S.; Khainovski, N.; Pillai, S.; Dey, S.; Daniels, S.; et al. Multiplexed Protein Quantitation in *Saccharomyces cerevisiae* Using Amine-reactive Isobaric Tagging Reagents. *Mol. Cell. Proteom.* **2004**, *3*, 1154–1169. [[CrossRef](#)] [[PubMed](#)]
5. Dayon, L.; Hainard, A.; Licker, V.; Turck, N.; Kuhn, K.; Hochstrasser, D.F.; Burkhard, P.R.; Sanchez, J.C. Relative quantification of proteins in human cerebrospinal fluids by MS/MS using 6-plex isobaric tags. *Anal. Chem.* **2008**, *80*, 2921–2931. [[CrossRef](#)]
6. McAlister, G.C.; Huttlin, E.L.; Haas, W.; Ting, L.; Jedrychowski, M.P.; Rogers, J.C.; Kuhn, K.; Pike, I.; Grothe, R.A.; Blethrow, J.D.; et al. Increasing the multiplexing capacity of TMTs using reporter ion isotopologues with isobaric masses. *Anal. Chem.* **2012**, *84*, 7469–7478. [[CrossRef](#)]
7. Potts, G.K.; Voigt, E.A.; Bailey, D.J.; Rose, C.M.; Westphall, M.S.; Hebert, A.S.; Yin, J.; Coon, J.J. Neucode Labels for Multiplexed, Absolute Protein Quantification. *Anal. Chem.* **2016**, *88*, 3295–3303. [[CrossRef](#)] [[PubMed](#)]
8. Thompson, A.; Wölmer, N.; Koncarevic, S.; Selzer, S.; Böhm, G.; Legner, H.; Schmid, P.; Kienle, S.; Penning, P.; Höhle, C.; et al. TMTpro: Design, Synthesis, and Initial Evaluation of a Proline-Based Isobaric 16-Plex Tandem Mass Tag Reagent Set. *Anal. Chem.* **2019**, *91*, 15941–15950. [[CrossRef](#)]
9. Li, J.; Van Vranken, J.G.; Pontano Vaites, L.; Schweppe, D.K.; Huttlin, E.L.; Etienne, C.; Nandhikonda, P.; Viner, R.; Robitaille, A.M.; Thompson, A.H.; et al. TMTpro reagents: A set of isobaric labeling mass tags enables simultaneous proteome-wide measurements across 16 samples. *Nat. Methods* **2020**, *17*, 399–404. [[CrossRef](#)]
10. Wang, Z.; Yu, K.; Tan, H.; Wu, Z.; Cho, J.-H.; Han, X.; Sun, H.; Beach, T.G.; Peng, J. 27-Plex Tandem Mass Tag Mass Spectrometry for Profiling Brain Proteome in Alzheimer's Disease. *Anal. Chem.* **2020**, *92*, 7162–7170. [[CrossRef](#)]
11. Ichou, F.; Schwarzenberg, A.; Lesage, D.; Alves, S.; Junot, C.; Machuron-Mandard, X.; Tabet, J.-C. Comparison of the activation time effects and the internal energy distributions for the CID, PQD and HCD excitation modes. *J. Mass Spectrom.* **2014**, *49*, 498–508. [[CrossRef](#)]
12. Nilsson, C.L. Advances in quantitative phosphoproteomics. *Anal. Chem.* **2012**, *84*, 735–746. [[CrossRef](#)] [[PubMed](#)]
13. Ruhaak, L.R.; Xu, G.; Li, Q.; Goonatilleke, E.; Lebrilla, C.B. Mass Spectrometry Approaches to Glycomic and Glycoproteomic Analyses. *Chem. Rev.* **2018**, *118*, 7886–7930. [[CrossRef](#)] [[PubMed](#)]
14. Rauniyar, N.; Yates, J.R. Isobaric labeling-based relative quantification in shotgun proteomics. *J. Proteome Res.* **2014**, *13*, 5293–5309. [[CrossRef](#)]
15. Reiding, K.R.; Bondt, A.; Franc, V.; Heck, A.J.R. The benefits of hybrid fragmentation methods for glycoproteomics. *TrAC Trends Anal. Chem.* **2018**, *108*, 260–268. [[CrossRef](#)]
16. Dang, L.; Jia, L.; Zhi, Y.; Li, P.; Zhao, T.; Zhu, B.; Lan, R.; Hu, Y.; Zhang, H.; Sun, S. Mapping human N-linked glycoproteins and glycosylation sites using mass spectrometry. *TrAC Trends Anal. Chem.* **2019**, *114*, 143–150. [[CrossRef](#)]
17. Liu, M.Q.; Zeng, W.F.; Fang, P.; Cao, W.Q.; Liu, C.; Yan, G.Q.; Zhang, Y.; Peng, C.; Wu, J.Q.; Zhang, X.J.; et al. PGlyco 2.0 enables precision N-glycoproteomics with comprehensive quality control and one-step mass spectrometry for intact glycopeptide identification. *Nat. Commun.* **2017**, *8*, 438. [[CrossRef](#)] [[PubMed](#)]
18. Cao, L.; Tolić, N.; Qu, Y.; Meng, D.; Zhao, R.; Zhang, Q.; Moore, R.J.; Zink, E.M.; Lipton, M.S.; Paša-Tolić, L.; et al. Characterization of intact N- and O-linked glycopeptides using higher energy collisional dissociation. *Anal. Biochem.* **2014**, *452*, 96–102. [[CrossRef](#)] [[PubMed](#)]
19. Xiao, K.; Tian, Z. Site- and Structure-Specific Quantitative N-Glycoproteomics Using RPLC-pentaHILIC Separation and the Intact N-Glycopeptide Search Engine GPSeeker. *Curr. Protoc. Protein Sci.* **2019**, *97*, e94. [[CrossRef](#)] [[PubMed](#)]
20. Yang, H.; Yang, C.; Sun, T. Characterization of glycopeptides using a stepped higher-energy C-trap dissociation approach on a hybrid quadrupole orbitrap. *Rapid Commun. Mass Spectrom.* **2018**, *32*, 1353–1362. [[CrossRef](#)]

21. Park, G.W.; Kim, J.H.J.Y.; Hwang, H.; Lee, J.Y.; Ahn, Y.H.; Lee, H.K.; Ji, E.S.; Kim, K.H.; Jeong, H.K.; Yun, K.N.; et al. Integrated GlycoProteome Analyzer (I-GPA) for Automated Identification and Quantitation of Site-Specific N-Glycosylation. *Sci. Rep.* **2016**, *6*, 21175. [[CrossRef](#)] [[PubMed](#)]
22. Riley, N.M.; Malaker, S.A.; Driessen, M.D.; Bertozzi, C.R. Optimal Dissociation Methods Differ for N- and O-Glycopeptides. *J. Proteome Res.* **2020**, *19*, 3286–3301. [[CrossRef](#)] [[PubMed](#)]
23. Ye, H.; Boyne, M.T.; Buhse, L.F.; Hill, J. Direct approach for qualitative and quantitative characterization of glycoproteins using tandem mass tags and an LTQ orbitrap XL electron transfer dissociation hybrid mass spectrometer. *Anal. Chem.* **2013**, *85*, 1531–1539. [[CrossRef](#)] [[PubMed](#)]
24. Zhu, H.; Qiu, C.; Ruth, A.C.; Keire, D.A.; Ye, H. A LC-MS All-in-One Workflow for Site-Specific Location, Identification and Quantification of N-/O- Glycosylation in Human Chorionic Gonadotropin Drug Products. *AAPS J.* **2017**, *19*, 846–855. [[CrossRef](#)] [[PubMed](#)]
25. Lee, H.J.; Cha, H.J.; Lim, J.S.; Lee, S.H.; Song, S.Y.; Kim, H.; Hancock, W.S.; Yoo, J.S.; Paik, Y.K. Abundance-ratio-based semiquantitative analysis of site-specific N-linked glycopeptides present in the plasma of hepatocellular carcinoma patients. *J. Proteome Res.* **2014**, *13*, 2328–2338. [[CrossRef](#)]
26. Shah, P.; Wang, X.; Yang, W.; Toghi Eshghi, S.; Sun, S.; Hoti, N.; Chen, L.; Yang, S.; Pasay, J.; Rubin, A.; et al. Integrated Proteomic and Glycoproteomic Analyses of Prostate Cancer Cells Reveal Glycoprotein Alteration in Protein Abundance and Glycosylation. *Mol. Cell. Proteom.* **2015**, *14*, 2753–2763. [[CrossRef](#)]
27. Chen, Z.; Yu, Q.; Hao, L.; Liu, F.; Johnson, J.; Tian, Z.; Kao, W.J.; Xu, W.; Li, L. Site-specific characterization and quantitation of N-glycopeptides in PKM2 knockout breast cancer cells using DiLeu isobaric tags enabled by electron-transfer/higher-energy collision dissociation (EThcD). *Analyst* **2018**, *143*, 2508–2519. [[CrossRef](#)]
28. Yu, Q.; Wang, B.; Chen, Z.; Urabe, G.; Glover, M.S.; Shi, X.; Guo, L.W.; Kent, K.C.; Li, L. Electron-Transfer/Higher-Energy Collision Dissociation (EThcD)-Enabled Intact Glycopeptide/Glycoproteome Characterization. *J. Am. Soc. Mass Spectrom.* **2017**, *28*, 1751–1764. [[CrossRef](#)]
29. Zhu, H.; Qiu, C.; Gryniewicz-Ruzicka, C.M.; Keire, D.A.; Ye, H. Multiplexed Comparative Analysis of Intact Glycopeptides Using Electron-Transfer Dissociation and Synchronous Precursor Selection Based Triple-Stage Mass Spectrometry. *Anal. Chem.* **2020**, *92*, 7547–7555. [[CrossRef](#)]
30. Potel, C.M.; Lemeer, S.; Heck, A.J.R. Phosphopeptide Fragmentation and Site Localization by Mass Spectrometry: An Update. *Anal. Chem.* **2019**, *91*, 126–141. [[CrossRef](#)]
31. Robinson, M.R.; Taliaferro, J.M.; Dalby, K.N.; Brodbelt, J.S. 193 Nm Ultraviolet Photodissociation Mass Spectrometry for Phosphopeptide Characterization in the Positive and Negative Ion Modes. *J. Proteome Res.* **2016**, *15*, 2739–2748. [[CrossRef](#)]
32. Ko, B.J.; Brodbelt, J.S. Comparison of glycopeptide fragmentation by collision induced dissociation and ultraviolet photodissociation. *Int. J. Mass Spectrom.* **2015**, *377*, 385–392. [[CrossRef](#)]
33. Madsen, J.A.; Ko, B.J.; Xu, H.; Iwashkiw, J.A.; Robotham, S.A.; Shaw, J.B.; Feldman, M.F.; Brodbelt, J.S. Concurrent Automated Sequencing of the Glycan and Peptide Portions of O -Linked Glycopeptide Anions by Ultraviolet Photodissociation Mass Spectrometry. *Anal. Chem.* **2013**, *85*, 9253–9261. [[CrossRef](#)] [[PubMed](#)]
34. Brodie, N.I.; Huguet, R.; Zhang, T.; Viner, R.; Zabrouskov, V.; Pan, J.; Petrotchenko, E.V.; Borchers, C.H. Top-Down Hydrogen-Deuterium Exchange Analysis of Protein Structures Using Ultraviolet Photodissociation. *Anal. Chem.* **2018**, *90*, 3079–3082. [[CrossRef](#)]
35. Shaw, J.B.; Malhan, N.; Vasil'Ev, Y.V.; Lopez, N.I.; Makarov, A.; Beckman, J.S.; Voinov, V.G. Sequencing Grade Tandem Mass Spectrometry for Top-Down Proteomics Using Hybrid Electron Capture Dissociation Methods in a Benchtop Orbitrap Mass Spectrometer. *Anal. Chem.* **2018**, *90*, 10819–10827. [[CrossRef](#)] [[PubMed](#)]
36. Morrison, L.J.; Brodbelt, J.S. Charge site assignment in native proteins by ultraviolet photodissociation (UVPD) mass spectrometry. *Analyst* **2016**, *141*, 166–176. [[CrossRef](#)]
37. Fort, K.L.; Dyachenko, A.; Potel, C.M.; Corradini, E.; Marino, F.; Barendregt, A.; Makarov, A.A.; Scheltema, R.A.; Heck, A.J.R. Implementation of Ultraviolet Photodissociation on a Benchtop Q Exactive Mass Spectrometer and Its Application to Phosphoproteomics. *Anal. Chem.* **2016**, *88*, 2303–2310. [[CrossRef](#)]
38. Morrison, L.J.; Brodbelt, J.S. 193 nm Ultraviolet Photodissociation Mass Spectrometry of Tetrameric Protein Complexes Provides Insight into Quaternary and Secondary Protein Topology. *J. Am. Chem. Soc.* **2016**, *138*, 10849–10859. [[CrossRef](#)] [[PubMed](#)]
39. Mehaffey, M.R.; Cammarata, M.B.; Brodbelt, J.S. Tracking the Catalytic Cycle of Adenylate Kinase by Ultraviolet Photodissociation Mass Spectrometry. *Anal. Chem.* **2018**, *90*, 839–846. [[CrossRef](#)]
40. Theisen, A.; Black, R.; Corinti, D.; Brown, J.M.; Bellina, B.; Barran, P.E. Initial Protein Unfolding Events in Ubiquitin, Cytochrome c and Myoglobin Are Revealed with the Use of 213 nm UVPD Coupled to IM-MS. *J. Am. Soc. Mass Spectrom.* **2019**, *30*, 24–33. [[CrossRef](#)]
41. Zhou, M.; Liu, W.; Shaw, J.B. Charge Movement and Structural Changes in the Gas-Phase Unfolding of Multimeric Protein Complexes Captured by Native Top-Down Mass Spectrometry. *Anal. Chem.* **2020**, *92*, 1788–1795. [[CrossRef](#)]
42. Escobar, E.E.; King, D.T.; Serrano-Negrón, J.E.; Alteen, M.G.; Vocadlo, D.J.; Brodbelt, J.S. Precision Mapping of O-Linked N-Acetylglucosamine Sites in Proteins Using Ultraviolet Photodissociation Mass Spectrometry. *J. Am. Chem. Soc.* **2020**, *142*, 11569–11577. [[CrossRef](#)] [[PubMed](#)]

43. Kim, S.; Pevzner, P.A. MS-GF+ makes progress towards a universal database search tool for proteomics. *Nat. Commun.* **2014**, *5*, 5277. [[CrossRef](#)] [[PubMed](#)]
44. Monroe, M.E.; Shaw, J.L.; Daly, D.S.; Adkins, J.N.; Smith, R.D. MASIC: A software program for fast quantitation and flexible visualization of chromatographic profiles from detected LC-MS(/MS) features. *Comput. Biol. Chem.* **2008**, *32*, 215–217. [[CrossRef](#)] [[PubMed](#)]
45. Park, J.; Piehowski, P.D.; Wilkins, C.; Zhou, M.; Mendoza, J.; Fujimoto, G.M.; Gibbons, B.C.; Shaw, J.B.; Shen, Y.; Shukla, A.K.; et al. Informed-Proteomics: Open-source software package for top-down proteomics. *Nat. Methods* **2017**, *14*, 909–914. [[CrossRef](#)] [[PubMed](#)]
46. Kronewitter, S.R.; Hyun, J.A.; De Leoz, M.L.; Lebrilla, C.B.; Miyamoto, S.; Leiserowitz, G.S. The development of retrosynthetic glycan libraries to profile and classify the human serum N-linked glycome. *Proteomics* **2009**, *9*, 2986–2994. [[CrossRef](#)]
47. Ozohanics, O.; Turiák, L.; Puerta, A.; Vékey, K.; Drahos, L. High-performance liquid chromatography coupled to mass spectrometry methodology for analyzing site-specific N-glycosylation patterns. *J. Chromatogr. A* **2012**, *1259*, 200–212. [[CrossRef](#)]
48. Lee, J.Y.; Lee, H.K.; Park, G.W.; Hwang, H.; Jeong, H.K.; Yun, K.N.; Ji, E.S.; Kim, K.H.; Kim, J.S.; Kim, J.W.; et al. Characterization of Site-Specific N-Glycopeptide Isoforms of α -1-Acid Glycoprotein from an Interlaboratory Study Using LC-MS/MS. *J. Proteome Res.* **2016**, *15*, 4146–4164. [[CrossRef](#)]
49. Holden, D.D.; Brodbelt, J.S. Improving Performance Metrics of Ultraviolet Photodissociation Mass Spectrometry by Selective Precursor Ejection. *Anal. Chem.* **2017**, *89*, 837–846. [[CrossRef](#)]
50. Parker, W.R.; Holden, D.D.; Cotham, V.C.; Xu, H.; Brodbelt, J.S. Cysteine-Selective Peptide Identification: Selenium-Based Chromophore for Selective S-Se Bond Cleavage with 266 nm Ultraviolet Photodissociation. *Anal. Chem.* **2016**, *88*, 7222–7229. [[CrossRef](#)]
51. Aponte, J.R.; Vasicek, L.; Swaminathan, J.; Xu, H.; Koag, M.C.; Lee, S.; Brodbelt, J.S. Streamlining bottom-up protein identification based on selective ultraviolet photodissociation (UVPD) of chromophore-tagged histidine-and tyrosine-containing peptides. *Anal. Chem.* **2014**, *86*, 6237–6244. [[CrossRef](#)]
52. Brodbelt, J.S. Photodissociation mass spectrometry: New tools for characterization of biological molecules. *Chem. Soc. Rev.* **2014**, *43*, 2757–2783. [[CrossRef](#)] [[PubMed](#)]
53. Wysocki, V.H.; Tsaprailis, G.; Smith, L.L.; Brexi, L.A. Mobile and localized protons: A framework for understanding peptide dissociation. *J. Mass Spectrom.* **2000**, *35*, 1399–1406. [[CrossRef](#)]
54. Brauman, J.I.; Riveros, J.M.; Blair, L.K. Gas-Phase Basicities of Amines. *J. Am. Chem. Soc.* **1971**, *93*, 3914–3916. [[CrossRef](#)]
55. Varki, A.; Cummings, R.D.; Esko, J.D.; Freeze, H.H.; Stanley, P.; Marth, J.D.; Bertozzi, C.R.; Hart, G.W.; Etzler, M.E. Symbol nomenclature for glycan representation. *Proteomics* **2009**, *9*, 5398–5399. [[CrossRef](#)] [[PubMed](#)]
56. Cupp-Sutton, K.A.; Wu, S. High-throughput quantitative top-down proteomics. *Mol. Omics* **2020**, *16*, 91–99. [[CrossRef](#)] [[PubMed](#)]